Article

CuCrO$_2$ Nanoparticles Incorporated into PTAA as a Hole Transport Layer for 85 °C and Light Stabilities in Perovskite Solar Cells

Bumjin Gil [1,†] , **Jinhyun Kim [1,†]** , **Alan Jiwan Yun [1]** , **Kimin Park [1]** , **Jaemin Cho [1]** , **Minjun Park [2]** **and Byungwoo Park [1,*]**

[1] Department of Materials Science and Engineering, Research Institute of Advanced Materials, Seoul National University, Seoul 08826, Korea; bestgil123@snu.ac.kr (B.G.); kim767@snu.ac.kr (J.K.); hangyeolee@snu.ac.kr (A.J.Y.); flamethrow@snu.ac.kr (K.P.); jjm7004@snu.ac.kr (J.C.)

[2] Department of Chemical Engineering, Ulsan National Institute of Science and Technology, Ulsan 44919, Korea; sia835@unist.ac.kr

* Correspondence: byungwoo@snu.ac.kr

† These authors contributed equally to this work.

check for updates

Abstract: High-mobility inorganic CuCrO$_2$ nanoparticles are co-utilized with conventional poly(bis(4-phenyl)(2,5,6-trimethylphenyl)amine) (PTAA) as a hole transport layer (HTL) for perovskite solar cells to improve device performance and long-term stability. Even though CuCrO$_2$ nanoparticles can be readily synthesized by hydrothermal reaction, it is difficult to form a uniform HTL with CuCrO$_2$ alone due to the severe agglomeration of nanoparticles. Herein, both CuCrO$_2$ nanoparticles and PTAA are sequentially deposited on perovskite by a simple spin-coating process, forming uniform HTL with excellent coverage. Due to the presence of high-mobility CuCrO$_2$ nanoparticles, CuCrO$_2$/PTAA HTL demonstrates better carrier extraction and transport. A reduction in trap density is also observed by trap-filled limited voltages and capacitance analyses. Incorporation of stable CuCrO$_2$ also contributes to the improved device stability under heat and light. Encapsulated perovskite solar cells with CuCrO$_2$/PTAA HTL retain their efficiency over 90% after ~900-h storage in 85 °C/85% relative humidity and under continuous 1-sun illumination at maximum-power point.

Keywords: perovskite solar cell; hole transport layer; CuCrO$_2$ nanoparticles; thermal stability; light stability

1. Introduction

In the field of next-generation photovoltaics, organic-inorganic hybrid halide perovskite solar cells have gathered tremendous attention since their emergence due to their rapidly growing power conversion efficiency (PCE), micrometer-scale carrier diffusion length, high absorption coefficient over solar spectrum regions, small exciton binding energy, etc. [1–11]. However, its relatively poor stability is still a main bottleneck toward commercialization, which becomes more serious at elevated temperatures or under constant illumination due to the rapid degradation of materials along with the accelerated formation and migration of defects [12–18]. One of the most vulnerable components is traditional organic small-molecule-based hole transport layers (HTL) such as 2,2′,7,7′-tetrakis(N,N-di-p-methoxyphenylamine)-9,9′-spirobifuorene (spiro-OMeTAD), which can easily decompose under the presence of heat [19,20]. Other candidates, such as poly(bis(4-phenyl)(2,5,6-trimethylphenyl)amine) (PTAA), are reported to be more durable in terms of stability [21–25], but diffusion of additives and ionic species can still occur to hamper the perovskite-HTL interface [26–29].

As an alternative to the unstable organic HTLs, inorganic HTLs such as CuSCN and various metal oxides have been shown to achieve long-term stability [30–44]. Among them, delafossite metal oxide $CuCrO_2$ is considered as one of the most promising candidates as an HTL due to its high mobility of 0.1–1 cm^2 V^{-1} s^{-1}, favorable band alignment with perovskite, and facile synthesis method of nanoparticles by hydrothermal reaction of nitrate-based precursors [45–51]. Several research groups have adopted $CuCrO_2$ HTL in a *p-i-n* structure to obtain ambient stability comparable to its organic counterparts [52–55]. However, few studies have utilized $CuCrO_2$ in an *n-i-p* structure, mainly due to its difficulty in forming a uniform film over the perovskite layer [56]. Studies demonstrating long-term stabilities under continuous heat or light are also lacking; thus, a lot of effort is still required to successfully utilize $CuCrO_2$ materials as a stable and efficient HTL.

One strategy to overcome the barrier of poor film formability of nanoparticle-type HTL is to co-utilize with other HTL that can form homogeneous precursor solutions, which can have multiple advantages over single-component solutions. The solution-based secondary HTL can successfully immerse between nanoparticles, which can greatly improve the film uniformity and thereby reduce surface/interface-related defects. The ability to utilize high-mobility nanoparticles can also improve the overall hole mobility of the HTL and the stability of the perovskite-HTL interface, especially when the solution-based HTL is known to be susceptible to the interfacial degradation. Several studies have demonstrated this hybrid-type design, such as NiO_x/spiro-OMeTAD, NiO_x/CuSCN, and $CuGaO_2$/CuSCN, indicating the potential for further improvement of HTL by this co-utilization approach [57–59].

In this work, hydrothermally synthesized $CuCrO_2$ nanoparticles are incorporated into the conventional PTAA to form $CuCrO_2$/PTAA hybrid HTL that can effectively reduce the surface roughness. The utilization of high-mobility and stable $CuCrO_2$ can boost the hole extraction while passivating deep-level traps, which are confirmed by optoelectronic analyses. Stabilities of ~900 h under 85 °C/85% relative humidity (RH) and continuous 1-sun illumination further confirm the successful durability of the bilayer HTL, suggesting a straightforward but effective method to improve the stabilities of perovskite solar cells.

2. Materials and Methods

2.1. Synthesis of CuCrO₂ Nanoparticles

$Cu(NO_3)_2 \cdot 2.5H_2O$ (Alfa Aesar, Heysham, UK) and $Cr(NO_3)_3 \cdot 9H_2O$ (Alfa Aesar, Heysham, UK) were dissolved in deionized water (DW) with concentration of 0.21 M each. After 15 min of stirring, 1.8 M of NaOH (Daejung, Siheung, Korea) was added, and the solution was stirred for another 15 min. Then, the solution was transferred to a Teflon-lined stainless-steel autoclave and placed in an oven with a temperature of 220 °C for 60 h. After the reaction, a dark-green precipitate containing $CuCrO_2$ nanoparticles was formed. The synthesized nanoparticles were centrifuged and sequentially washed with 1 N HCl (Daejung, Siheung, Korea) and isopropyl alcohol (IPA, Daejung, Siheung, Korea) four times, and stored in IPA for future use.

2.2. Device Fabrication

Glasses coated with indium-doped tin oxide (ITO) were cleaned in acetone (Daejung, Siheung, Korea), ethanol (Daejung, Siheung, Korea), and DW for 15 min each by sonication, followed by UV-ozone treatment for 15 min. For the electron transport layer, SnO_2 aqueous colloidal dispersion (Alfa Aesar, Heysham, UK) was diluted by DW to 2.5 wt. %, spin-coated on ITO at 3000 rpm for 30 s, and annealed at 120 °C for 30 min. Perovskite precursor solution of 1.3 M $Cs_{0.05}(FA_{0.85}MA_{0.15})_{0.95}Pb(I_{0.85}Br_{0.15})_3$ (FA and MA stand for formamidinium and methylammonium, respectively) was fabricated by dissolving PbI_2 (TCI, Fukaya, Japan), $PbBr_2$ (TCI, Fukaya, Japan), FAI (Greatcell Solar, Queanbeyan, Australia), MABr (Greatcell Solar, Queanbeyan, Australia), and CsI (TCI, Fukaya, Japan) with desired ratio in a 4:1 (*v/v*) mixture of N,N-dimethylformamide (DMF, Sigma-Aldrich, St. Louis, MO, USA) and dimethyl

sulfoxide (DMSO, Sigma-Aldrich, St. Louis, MO, USA). In a N_2-filled glovebox, the perovskite solution was deposited on a SnO_2 layer by spin-coating at 1000 rpm for 10 s, followed by 5000 rpm for 20 s. A total of 300 μL of chlorobenzene (Sigma-Aldrich, St. Louis, MO, USA) was dripped onto the spinning substrate 3 s before the end of the spin-coating process. The samples were then annealed at 100 °C for 40 min. For the $CuCrO_2$ hole transport layer, the stored $CuCrO_2$ nanoparticle dispersion was further diluted by IPA to the desired concentrations (0.5–3 mg mL^{-1}), subjected to sonication for 1 h, and spin-coated at 5000 rpm for 30 s, followed by annealing at 50 °C for 10 min to remove residual solvent. For a $CuCrO_2$-only device, the spin-coating steps were repeated multiple times to obtain full coverage of HTL, whereas for a $CuCrO_2$/PTAA device, single spin-coating of $CuCrO_2$ was sufficient. For the PTAA hole transport layer, solution was fabricated by dissolving 20 mg of PTAA (47 kDa, MS Solutions, Seoul, Korea) in 1 mL of chlorobenzene, with the addition of 6 μL of 4-*tert*-butylpyridine (Sigma-Aldrich, St. Louis, MO, USA) and 4 μL of 520 mg mL^{-1} bis(trifluoromethane)sulfonimide lithium salt (Sigma-Aldrich, St. Louis, MO, USA) solution in acetonitrile (Sigma-Aldrich, St. Louis, MO, USA). The PTAA solution was then spin-coated on either perovskite film or pre-deposited $CuCrO_2$ film at 3000 rpm for 30 s. Finally, an Au electrode was deposited by thermal evaporation. For encapsulated devices, the devices were sealed with cover glass using UV-curable epoxy resin (Nagase, Osaka, Japan).

2.3. Characterization

X-ray diffraction was conducted using a diffractometer (New D8 Advance, Bruker, Billerica, MA, USA). Surface roughness of the film was analyzed by an atomic force microscope (NX-10, Park Systems, Suwon, Korea). The cross-sectional image of an HTL film was obtained by a field-emission scanning electron microscope (Merlin-Compact, Zeiss, Oberkochen, Germany). The optical bandgap was analyzed by UV-visible absorption spectroscopy using a spectrophotometer (V-770, JASCO, Easton, MD, USA). A time-of-flight secondary ion mass spectrometer (TOF-SIMS-5, IONTOF, Münster, Germany) was utilized to obtain the depth profile of the device. Photoluminescence (LabRam HV Evolution, Horiba, Kyoto, Japan) and time-resolved photoluminescence (FluoTime 300, Picoquant, Berlin, Germany) of the films were analyzed using lasers with excitation wavelengths of 523 nm and 398 nm, respectively. Space-charge limited current (SCLC) and admittance analyses were conducted using a potentiostat (Zive SP-1, WonATech, Seoul, Korea), where dark current was measured under varying direct current (DC) bias for SCLC measurement and impedance was measured at a frequency of 10^{-2}–10^4 Hz using 10 mV AC voltage perturbation for admittance analysis. J-V curves of the solar cells were obtained using a solar simulator (K3000, McScience, Suwon, Korea) with 1-sun (AM 1.5G) illumination on the glass/ITO side, with a voltage sweep between 1.2 and −0.1 V, a scan rate of 100 mV s^{-1}, and active areas for solar cells were 0.09 cm^2. For the thermal stability test, encapsulated devices were stored within a dark test chamber (TH-PE-025, JeioTech, Daejeon, Korea) with controlled temperature and humidity (85 °C/85% RH), and J-V scans of devices were periodically conducted. For the light stability test, encapsulated devices were tested with maximum-power-point tracking equipment (K3600, McScience, Suwon, Korea) under continuous 1-sun illumination, where maximum-power voltage is constantly applied to the cells during the test.

3. Results and Discussion

One of the prerequisites for HTL in an *n-i-p* type perovskite solar cell is continuous film formability that can yield a thin and compact layer above a perovskite substrate. The $CuCrO_2$/PTAA HTL deposited on the conventional triple-cation perovskite ($Cs_{0.05}(FA_{0.85}MA_{0.15})_{0.95}Pb(I_{0.85}Br_{0.15})_3$) displayed a smooth surface topography with reasonably small surface roughness (Figure 1a). However, due to the agglomeration of $CuCrO_2$ nanoparticles when deposited on perovskite substrate, simple one-step spin-coating of $CuCrO_2$ nanoparticles alone often yielded incomplete coverage; hence, multiple spin-coatings were required for $CuCrO_2$ to fully cover the underlying perovskite layer (Figure S1a,b). Moreover, even though the full coverage was obtained with only $CuCrO_2$, the resulting HTL displayed a much larger surface roughness compared to the $CuCrO_2$/PTAA, resulting in a low PCE (Figure 1b

and Figure S1c). The difficulty in creating a uniform film with nanoparticles alone suggests that incorporating a small number of nanoparticles within other solution-processable HTL is more suitable to utilize high-mobility nanoparticles, as suggested in this work. As shown in the cross-sectional image in Figure 1c, the final $CuCrO_2$/PTAA bilayer showed compact and dense morphology with ~100 nm thickness, suggesting that the PTAA solution was effectively wetted and immersed among the $CuCrO_2$ nanoparticles, and thereby formed a uniform film without any visible structural imperfections. Further analyses by x-ray diffraction (XRD) revealed that hydrothermally synthesized $CuCrO_2$ nanoparticles consisted of a mixture of desirable rhombohedral and hexagonal delafossite phases without any detectable impurities (Figure S2a) [52], and the perovskite layer was not damaged or decomposed into impurities like PbI_2 after the deposition of $CuCrO_2$/PTAA HTL (Figure S2b).
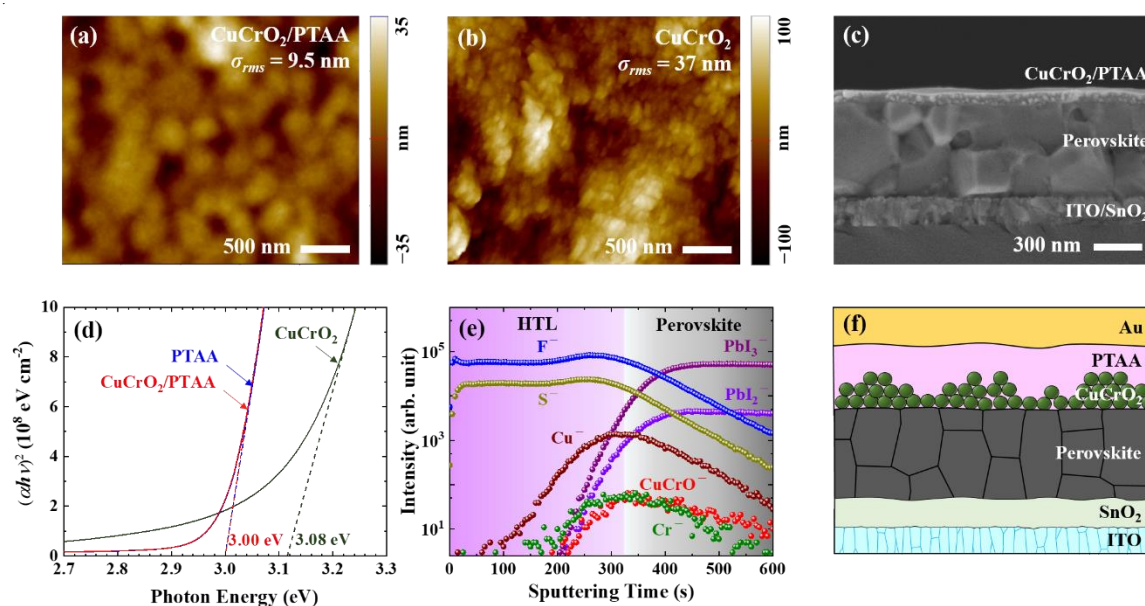

Figure 1. Morphological and structural analyses of $CuCrO_2$/PTAA and $CuCrO_2$ hole transport layer (HTL): (**a,b**) Topography and root-mean-square (RMS) surface roughness of each HTL deposited on indium-doped tin oxide (ITO)/SnO_2/perovskite, obtained by atomic force microscope (AFM); (**c**) Cross-sectional scanning electron microscopy (SEM) image of ITO/SnO_2/perovskite/HTL film; (**d**) UV-visible absorption spectra and the optical bandgap energy of each HTL deposited on a glass substrate; (**e**) Time-of-flight secondary ion mass spectrometry (TOF-SIMS) depth profile of the ITO/SnO_2/perovskite/$CuCrO_2$/PTAA film; (**f**) Schematic illustration of the device architecture with $CuCrO_2$/PTAA HTL. Light is incident on an ITO side during the solar cell operation.

The optical bandgap was determined to be 3.00 eV and 3.08 eV for PTAA-only and $CuCrO_2$-only HTL, respectively, as presented in Figure 1d [45,46,48–50,60,61]. The absorption spectrum and bandgap of the optimized $CuCrO_2$/PTAA layer were almost identical to those of PTAA, since a small number of $CuCrO_2$ nanoparticles was enough to form an effective and stable HTL layer. The presence and distribution of $CuCrO_2$ in the bilayer HTL was further confirmed by a time-of-flight secondary ion mass spectroscopy (TOF-SIMS), as shown in Figure 1e. PbI_2^- and PbI_3^- originated from the perovskite, and F^- and S^- originated from the additives of PTAA. Since species containing Cu and Cr were distributed near the perovskite-HTL interface, the $CuCrO_2$ nanoparticles were mainly located at the bottom part of the HTL, where they were percolated by the solution-processed PTAA (Figure 1f).

The electronic properties of $CuCrO_2$/PTAA hybrid HTL were investigated to evaluate its ability to extract and transport holes. Photoluminescence (PL) spectra in Figure 2a show that $CuCrO_2$/PTAA HTL exhibited slightly larger PL quenching compared to the bare PTAA, implying the increased hole-extracting ability due to the incorporation of high-mobility $CuCrO_2$ nanoparticles. Time-resolved PL spectra, as seen in Figure 2b, exhibited faster early-stage decay with $CuCrO_2$/PTAA compared to

PTAA, 14 vs. 28 ns, respectively [62–64]. To characterize the hole-extracting mobility more quantitatively, dark current-voltage (J-V) characteristics under DC bias were examined for the SCLC region with the ITO/HTL/Au structure (Figure 2c) [65,66]. The hole mobilities were 2.6×10^{-3} and 1.2×10^{-3} cm^2 V^{-1} s^{-1} for CuCrO$_2$/PTAA and bare PTAA, respectively, further supporting the role of high-mobility CuCrO$_2$ nanoparticles which enable faster hole extraction from the perovskite along the HTL.
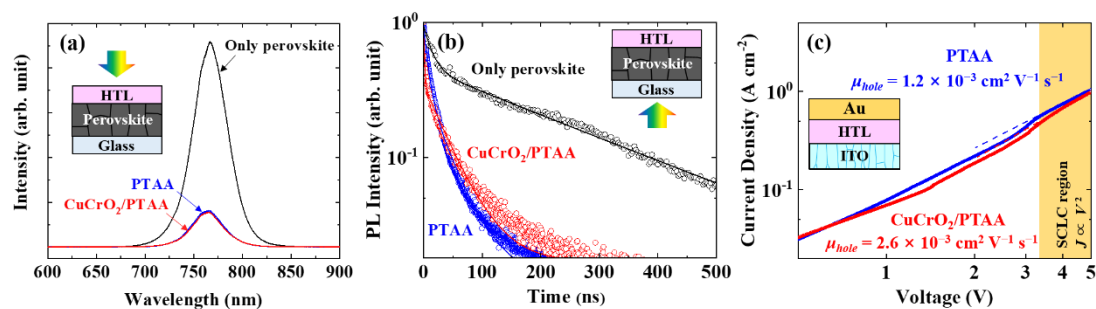

Figure 2. Electronic properties of CuCrO$_2$/PTAA HTL: (**a**) Steady-state photoluminescence (PL) and (**b**) time-resolved PL spectra (398-nm excitation with fitting lines) of bare perovskite and perovskite/HTL films deposited on glass; (**c**) Dark J-V characteristics of ITO/HTL/Au layers with different HTLs, where space-charge limited current (SCLC) region is indicated.

Next, the effect of CuCrO$_2$ incorporation into PTAA on the defect characteristics of the devices is discussed. Figure 3a shows dark J-V characteristics of hole-only devices with the structure of ITO/PTAA/perovskite/HTL/Au, with the upper HTL being either PTAA or CuCrO$_2$/PTAA. The trap-filled limited voltages (V_{TFL}) are related to the trap densities of the devices (N_t^{TFL}), exhibiting 6.6×10^{15} and 1.1×10^{16} cm^{-3} for the CuCrO$_2$/PTAA and bare PTAA, respectively [67]. Defect densities were also analyzed by capacitance analyses on the conventional ITO/SnO$_2$/perovskite/HTL/Au solar-cell structures. Nyquist plots in Figure 3b show larger semicircles for the device with CuCrO$_2$/PTAA compared to the PTAA, implying the increased recombination resistance which may be related to the decreased trap sites along the perovskite-HTL region [68–71]. It can also be seen in Figure 3c that two devices show different capacitive responses at low frequencies, indicating differences in the midgap trap states [68,72,73]. The trap density of states derived from the derivative of the capacitance (Figure 3d) exhibited a lower density of states in CuCrO$_2$/PTAA HTL, resulting in an almost halved integrated trap density (N_t^C) compared to the PTAA HTL [74–76]. These combined results of trap reduction suggest that CuCrO$_2$ nanoparticles near the perovskite-HTL interface surely passivate defects and related trap states, which can also contribute to the improvement of charge transport, as previously mentioned.

Solar cells with the device structure of ITO/SnO$_2$/perovskite/HTL/Au were fabricated with either CuCrO$_2$/PTAA or PTAA. With the optimum concentration of CuCrO$_2$ nanoparticles (Figure S3a), the champion cell yielded V_{OC} = 1.02 V, J_{SC} = 22.8 mA cm^{-2} and FF = 0.75 (PCE of 17.4%), whereas the bare PTAA yielded V_{OC} = 1.02 V, J_{SC} = 22.4 mA cm^{-2} and FF = 0.74 (PCE of 16.9%), as shown in Figure 4a (with the device parameters for multiple cells presented in Table 1 and Figure S3). While the external quantum efficiencies (EQEs) of the devices were quite similar (Figure 4c), the response at a longer wavelength (~700 nm or ~1.7 eV) exhibited better efficiency with the CuCrO$_2$-nanoparticle device, indicating an improved hole carrier collection, consistent with Figures 2 and 3. This improved hole collectivity might contribute to the increase of average J_{SC}, whereas the slight increases in trap-dependent parameters such as V_{OC} and FF further confirm the defect passivation effect by CuCrO$_2$ nanoparticles at the perovskite-HTL interface [77,78].
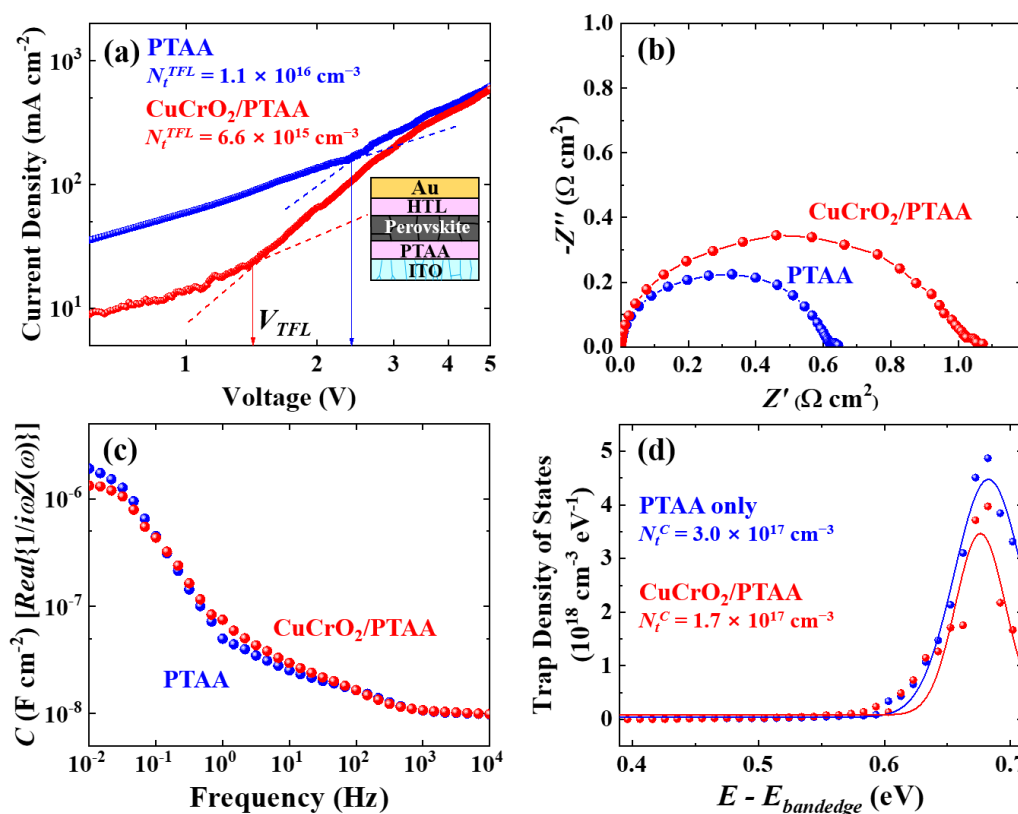
Figure 3. Trap density analyses of devices with different HTLs: (**a**) Dark J-V characteristics of hole-only devices with different upper HTLs, and calculated trap densities (N_t^{TFL}) from trap-filled limited voltages (V_{TFL}); (**b**) Nyquist plot, (**c**) capacitance-frequency plot, and (**d**) trap density of states obtained from the capacitances (with the integrated trap density N_t^C), in the device structure of $ITO/SnO_2/perovskite/HTL/Au$.
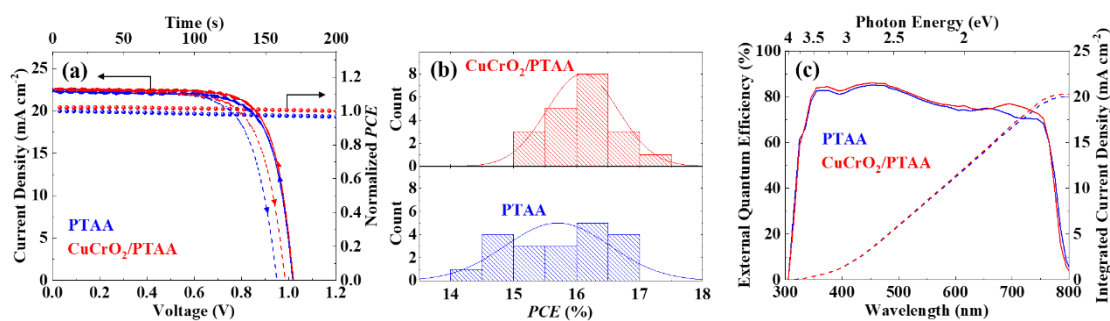

Figure 4. Photovoltaic performances of perovskite solar cells with $CuCrO_2/PTAA$ or PTAA as HTL: (**a**) J-V curves of champion cells and their steady-state efficiencies under maximum power voltage; (**b**) PCE distributions for 20 cells at each condition; (**c**) External quantum efficiency (EQE) of solar cells.

Table 1. Photovoltaic parameters of the solar cells (reverse scan for 20 cells). The data in parentheses are from the cells with the best power conversion efficiency (PCE).

HTL	V_{OC} (V)	J_{SC} (mA cm^{-2})	FF	PCE (%)	HI $(1-\eta_{FOR}/\eta_{REV})$ [1]
PTAA	1.02 ± 0.03 (1.02)	21.3 ± 1.1 (22.4)	0.72 ± 0.02 (0.74)	15.7 ± 0.8 (16.9)	0.09 ± 0.04
$CuCrO_2/PTAA$	1.03 ± 0.15 (1.02)	21.6 ± 3.3 (22.8)	0.73 ± 0.11 (0.75)	16.1 ± 2.4 (17.4)	0.11 ± 0.04

[1] HI, η_{FOR} and η_{REV} refer to the hysteresis index, forward-scan PCE and reverse-scan PCE, respectively.

The effect of $CuCrO_2$ nanoparticles on both thermal and light stabilities of the solar cells were also investigated. For thermal stability, encapsulated devices were stored under standard damp heat conditions (85 °C/85% relative humidity (RH)) [25,79,80], where encapsulation was applied to block other external degradation factors than heat. High humidity was used to detect devices with damaged encapsulation which would undergo rapid moisture-induced degradation with a leak. As presented in Figure 5, improved thermal stability was observed for the device with $CuCrO_2$/PTAA HTL, where the device maintained over 90% of its initial PCE after 860 h. The degradation of organic cations in the perovskite or small organic molecules within HTL can critically damage both bulk and the interface, especially at an elevated temperature [9,10,20,81,82]. It can be inferred that the presence of more heat-resistant $CuCrO_2$ nanoparticles in the vicinity of perovskite and HTL creates a more heat-resistant interface with reduced interfacial reactions to maintain excellent thermal stability.
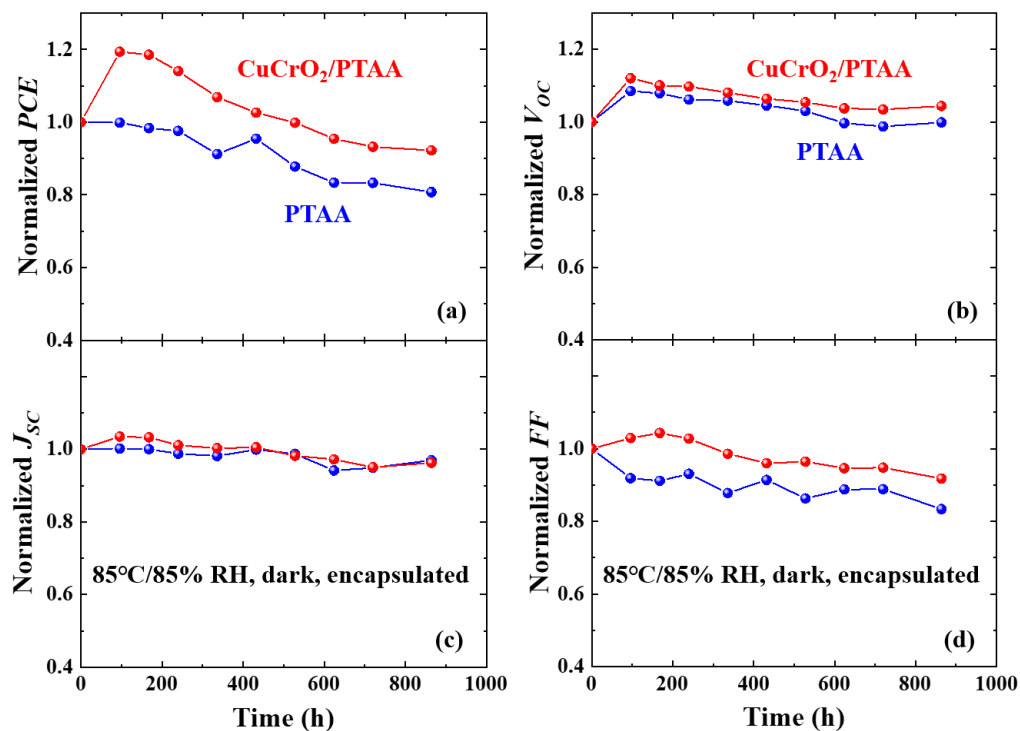
Figure 5. Thermal stabilities of solar cells with $CuCrO_2$/PTAA or PTAA HTL: Normalized values of (**a**) efficiency, (**b**) V_{OC}, (**c**) J_{SC}, and (**d**) FF of the encapsulated solar cells stored under 85 °C/85% relative humidity (RH) dark condition.

Light stabilities were tested by maximum-power-point tracking (MPPT) under continuous 1-sun (AM 1.5G) illumination. Figure 6 shows that a solar cell adopting $CuCrO_2$/PTAA HTL retains almost the entirety of its initial PCE after 960 h of operation, demonstrating superior light stability over the bare-PTAA device. Migration of halide defects as well as Li^+ from the additive in PTAA can accumulate at the perovskite-HTL interface and trigger interfacial degradation under operation conditions [15,28,29,83]. The improved light stability confirms that $CuCrO_2$ nanoparticles can directly prevent potential accumulation of traps at the interface, resulting in superior solar cells.
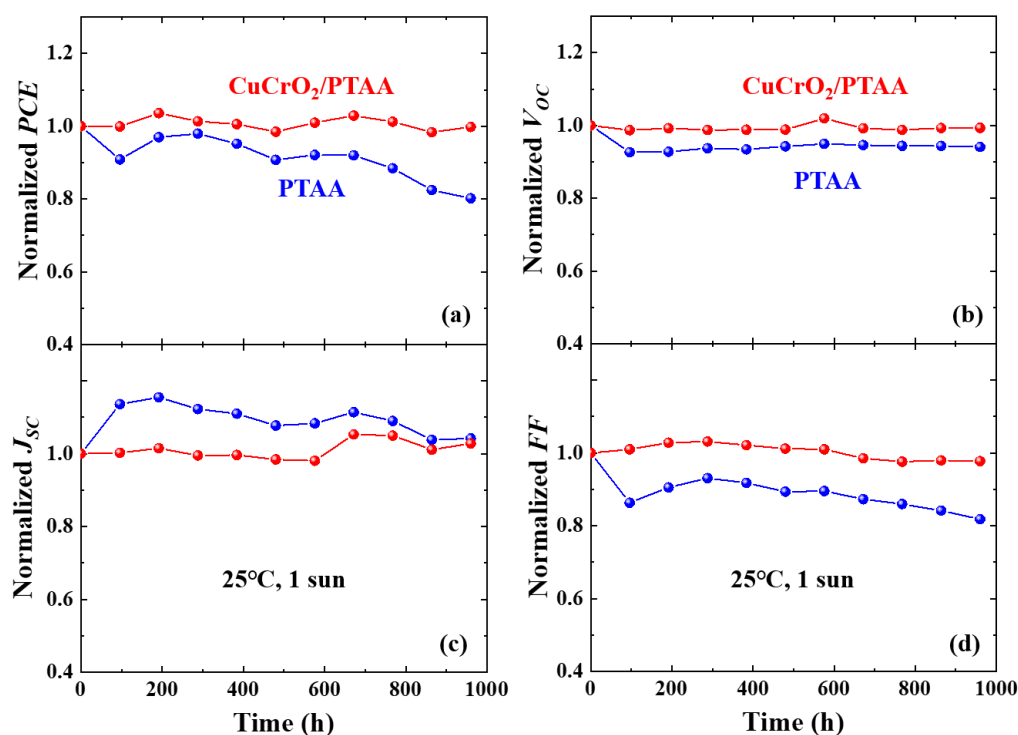
Figure 6. Light stabilities of solar cells with $CuCrO_2$/PTAA or PTAA HTL: Normalized values of (**a**) efficiency, (**b**) V_{OC}, (**c**) J_{SC}, and (**d**) FF of the encapsulated solar cells obtained by maximum-power-point tracking (MPPT) under continuous illumination of AM 1.5G at 25 °C.

4. Conclusions

Hybrid HTL, consisting of high-mobility $CuCrO_2$ nanoparticles embedded between perovskite and PTAA, was facilely adopted in the perovskite solar cells to guarantee excellent thermal and light stabilities. By a simple solution process, $CuCrO_2$/PTAA HTL was fabricated, yielding a uniform and smooth morphology. With $CuCrO_2$ nanoparticles providing high-mobility charge transport paths, $CuCrO_2$/PTAA HTL demonstrated more efficient hole-extraction abilities than the bare PTAA, and trap density was reduced by nearly half with $CuCrO_2$ nanoparticles. Therefore, solar cells with bilayer $CuCrO_2$/PTAA yielded higher PCE than the conventional PTAA-based ones, and also maintained over 90% of the initial efficiencies after storage under 85 °C/85% RH or operating under 1-sun MPPT for ~900 h. Our novel design of organic-inorganic hybrid HTL can aid in developing perovskite-based devices with improved hole extractability and reduced defects/traps, which ultimately leads to the superior stabilities under thermally induced and light-induced conditions.

Author Contributions: Conceptualization, B.G., J.K., and B.P.; methodology, B.G. and J.K.; validation, A.J.Y., K.P., J.C., M.P., and B.P.; formal analysis, B.G., J.K., A.J.Y., and K.P.; investigation, B.G. and J.K.; resources, A.J.Y., K.P., J.C., and M.P.; data curation, B.G. and J.K.; writing—original draft preparation, B.G., J.K., and B.P.; writing—review and editing, A.J.Y., K.P., J.C., M.P., and B.P.; supervision, B.P.; project administration, B.P.; funding acquisition, B.P. All authors have read and agreed to the published version of the manuscript.

Conflicts of Interest: The authors declare no conflict of interest.

References

1. Hodes, G. Perovskite-based solar cells. *Science* **2013**, *312*, 317–318. [CrossRef] [PubMed]
2. Snaith, H.J. Perovskites: The emergence of a new era for low-cost, high-efficiency solar cells. *J. Phys. Chem. Lett.* **2013**, *4*, 3623–3630. [CrossRef]
3. Stranks, S.D.; Eperon, G.E.; Grancini, G.; Menelaou, C.; Alcocer, M.J.P.; Leijtens, T.; Herz, L.M.; Petrozza, A.; Snaith, H.J. Electron-hole diffusion lengths exceeding 1 micrometer in an organometal trihalide perovskite absorber. *Science* **2013**, *342*, 341–344. [CrossRef]
4. Frost, J.M.; Butler, K.T.; Brivio, F.; Hendon, C.H.; Schilfgaarde, M.V.; Walsh, A. Atomistic origins of high-performance in hybrid halide perovskite solar cells. *Nano Lett.* **2014**, *14*, 2584–2590. [CrossRef] [PubMed]
5. Todorov, T.; Gershon, T.; Gunawan, O.; Lee, Y.S.; Sturdevant, S.; Chang, L.-Y.; Guha, S. Monolithic perovskite-CIGS tandem solar cells via in situ band gap engineering. *Adv. Energy Mater.* **2015**, *5*, 1500799. [CrossRef]
6. Park, N.-G. Perovskite solar cells: An emerging photovoltaic technology. *Mater. Today* **2015**, *18*, 65–72. [CrossRef]
7. Saliba, M.; Matsui, T.; Seo, J.-Y.; Domanski, K.; Correa-Baena, J.-P.; Nazeeruddin, M.K.; Zakeeruddin, S.M.; Tress, W.; Abate, A.; Hagfeldt, A.; et al. Cesium-containing triple cation perovskite solar cells: Improved stability, reproducibility and high efficiency. *Energy Environ. Sci.* **2016**, *9*, 1989–1997. [CrossRef]
8. Hwang, T.; Lee, B.; Kim, J.; Lee, S.; Gil, B.; Yun, A.J.; Park, B. From nanostructural evolution to dynamic interplay of constituents: Perspectives for perovskite solar cells. *Adv. Mater.* **2018**, *30*, 1704208. [CrossRef]
9. Kim, J.; Hwang, T.; Lee, B.; Lee, S.; Park, K.; Park, H.H.; Park, B. An aromatic diamine molecule as the *a*-site solute for highly durable and efficient perovskite solar cells. *Small Methods* **2019**, *3*, 1800361. [CrossRef]
10. Kim, J.; Yun, A.J.; Gil, B.; Lee, Y.; Park, B. Triamine-based aromatic cation as a novel stabilizer for efficient perovskite solar cells. *Adv. Funct. Mater.* **2019**, *29*, 1905190. [CrossRef]
11. Yang, A.; Blancon, J.-C.; Jiang, W.; Zhang, H.; Wong, J.; Yan, E.; Lin, Y.-R.; Crochet, J.; Kanatzidis, M.G.; Jariwala, D.; et al. Giant enhancement of photoluminescence emission in WS_2-two-dimensional perovskite heterostructures. *Nano Lett.* **2019**, *19*, 4852–4860. [CrossRef]
12. Fu, R.; Zhou, W.; Li, Q.; Zhao, Y.; Yu, D.; Zhao, Q. Stability challenges for perovskite solar cells. *ChemNanoMat* **2018**, *5*, 253–265. [CrossRef]
13. Gholipour, S.; Saliba, M. From exceptional properties to stability challenges of perovskite solar cells. *Small* **2018**, *14*, 1802385. [CrossRef] [PubMed]
14. Azpiroz, J.M.; Mosconi, E.; Bisquert, J.; De Angelis, F. Defect migration in methylammonium lead iodide and its role in perovskite solar cell operation. *Energy Environ. Sci.* **2015**, *8*, 2118–2127. [CrossRef]
15. Ruan, S.; Surmiak, M.-A.; Ruan, Y.; McMeekin, D.P.; Ebendorff-Heidepriem, H.; Cheng, Y.-B.; Lu, J.; McNeill, C.R. Light induced degradation in mixed-halide perovskites. *J. Mater. Chem. C* **2019**, *7*, 9326–9334. [CrossRef]
16. Holovský, J.; Amalathas, A.P.; Landová, L.; Dzurňák, B.; Conrad, B.; Ledinský, M.; Hájková, Z.; Pop-Georgievski, O.; Svoboda, J.; Yang, T.C.-J.; et al. Lead halide residue as a source of light-induced reversible defects in hybrid perovskite layers and solar cells. *ACS Energy Lett.* **2019**, *4*, 3011–3017. [CrossRef]
17. Park, C.-G.; Choi, W.-G.; Na, S.; Moon, T. All-inorganic perovskite $cspbi_2br$ through co-evaporation for planar heterojunction solar cells. *Electron. Mater. Lett.* **2019**, *15*, 56–60. [CrossRef]
18. Park, H.H.; Kim, J.; Kim, G.; Jung, H.; Kim, S.; Moon, C.S.; Lee, S.J.; Shin, S.S.; Hao, X.; Yun, J.S.; et al. Transparent electrodes consisting of a surface-treated buffer layer based on tungsten oxide for semitransparent perovskite solar cells and four-terminal tandem applications. *Small Methods* **2020**, *4*, 2070018. [CrossRef]
19. Malinauskas, T.; Tomkute-Luksiene, D.; Sens, R.; Daskeviciene, M.; Send, R.; Wonneberger, H.; Jankauskas, V.; Bruder, I.; Getautis, V. Enhancing thermal stability and lifetime of solid-state dye-sensitized solar cells via molecular engineering of the hole-transporting material spiro-OMeTAD. *ACS Appl. Mater. Interfaces* **2015**, *7*, 11107–11116. [CrossRef]
20. Jena, A.K.; Numata, Y.; Ikegamia, M.; Miyasaka, T. Role of spiro-OMeTAD in performance deterioration of perovskite solar cells at high temperature and reuse of the perovskite films to avoid Pb-Waste. *J. Mater. Chem. A* **2018**, *6*, 2219–2230. [CrossRef]
21. Ahn, N.; Jeon, I.; Yoon, J.; Kauppinen, E.I.; Matsuo, Y.; Maruyama, S.; Choi, M. Carbon-sandwiched perovskite solar cell. *J. Mater. Chem. A* **2018**, *6*, 1382–1389. [CrossRef]

22. Duong, T.; Wu, Y.; Shen, H.; Peng, J.; Wu, N.; White, T.; Weber, K.; Catchpole, K. Impact of light on the thermal stability of perovskite solar cells and development of stable semi-transparent cells. In Proceedings of the 2018 IEEE 7th World Conference on Photovoltaic Energy Conversion (WCPEC) (A Joint Conference of 45th IEEE PVSC, 28th PVSEC & 34th EU PVSEC), Waikoloa Village, HI, USA, 10–15 June 2018; pp. 3506–3508. [CrossRef]

23. Thote, A.; Jeon, I.; Lee, J.-W.; Seo, S.; Lin, H.-S.; Yang, Y.; Daiguji, H.; Maruyama, S.; Matsuo, Y. Stable and reproducible 2D/3D formamidinium-lead-iodide perovskite solar cells. *ACS Appl. Energy Mater.* **2019**, *2*, 2486–2493. [CrossRef]

24. Zhao, Q.; Wu, R.; Zhang, Z.; Xiong, J.; He, Z.; Fan, B.; Dai, Z.; Yang, B.; Xue, X.; Cai, P.; et al. Achieving efficient inverted planar perovskite solar cells with nondoped PTAA as a hole transport layer. *Org. Electron.* **2019**, *71*, 106–112. [CrossRef]

25. Matsui, T.; Yamamoto, T.; Nishihara, T.; Morisawa, R.; Yokoyama, T.; Sekiguchi, T.; Negami, T. Compositional engineering for thermally stable, highly efficient perovskite solar cells exceeding 20% power conversion efficiency with 85 °C/85% 1000 h stability. *Adv. Mater.* **2019**, *31*, 1806823. [CrossRef] [PubMed]

26. Berhe, T.A.; Su, W.-N.; Chen, C.-H.; Pan, C.-J.; Cheng, J.-H.; Chen, H.-M.; Tsai, M.-C.; Chen, L.-Y.; Dubale, A.A.; Hwang, B.-J. Organometal halide perovskite solar cells: Degradation and stability. *Energy Environ. Sci.* **2016**, *9*, 323–356. [CrossRef]

27. Kim, G.-W.; Kang, G.; Kim, J.; Lee, G.-Y.; Kim, H.I.; Pyeon, L.; Lee, J.; Park, T. Dopant-free polymeric hole transport materials for highly efficient and stable perovskite solar cells. *Energy Environ. Sci.* **2016**, *9*, 2326–2333. [CrossRef]

28. Yang, T.-Y.; Jeon, N.J.; Shin, H.-W.; Shin, S.S.; Kim, Y.Y.; Seo, J. achieving long-term operational stability of perovskite solar cells with a stabilized efficiency exceeding 20% after 1000 h. *Adv. Sci.* **2019**, *6*, 1900528. [CrossRef]

29. Schloemer, T.H.; Christians, J.A.; Luther, J.M.; Sellinger, A. Doping strategies for small molecule organic hole-transport materials: Impacts on perovskite solar cell performance and stability. *Chem. Sci.* **2019**, *10*, 1904–1935. [CrossRef]

30. Chen, J.; Park, N. Inorganic hole transporting materials for stable and high efficiency perovskite solar cells. *J. Phys. Chem. C* **2018**, *122*, 14039–14063. [CrossRef]

31. Gil, B.; Yun, A.J.; Lee, Y.; Kim, J.; Lee, B.; Park, B. Recent progress in inorganic hole transport materials for efficient and stable perovskite solar cells. *Electron. Mater. Lett.* **2019**, *15*, 505–524. [CrossRef]

32. Arora, N.; Dar, M.I.; Hinderhofer, A.; Pellet, N.; Schreiber, F.; Zakeeruddin, S.M.; Grätzel, M. Perovskite solar cells with CuSCN hole extraction layers yield stabilized efficiencies greater than 20%. *Science* **2017**, *358*, 768–771. [CrossRef] [PubMed]

33. Yue, S.; Liu, K.; Xu, R.; Li, M.; Azam, M.; Ren, K.; Liu, J.; Sun, Y.; Wang, Z.; Cao, D.; et al. Efficacious engineering on charge extraction for realizing highly efficient perovskite solar cells. *Energy Environ. Sci.* **2017**, *10*, 2570–2578. [CrossRef]

34. Wilson, S.S.; Bosco, J.P.; Tolstova, Y.; Scanlon, D.O.; Watson, G.W.; Atwater, H.A. Interface stoichiometry control to improve device voltage and modify band alignment in ZnO/Cu_2O heterojunction solar cells. *Energy Environ. Sci.* **2014**, *7*, 3606–3610. [CrossRef]

35. Lien, H.-T.; Wong, D.P.; Tsao, N.-H.; Huang, C.-I.; Su, C.; Chen, K.-H.; Chen, L.-C. Effect of copper oxide oxidation state on the polymer-based solar cell buffer layers. *ACS Appl. Mater. Interfaces* **2014**, *6*, 22445–22450. [CrossRef] [PubMed]

36. Rao, H.; Ye, S.; Sun, W.; Yan, W.; Li, Y.; Peng, H.; Liu, Z.; Bian, Z.; Li, Y.; Huang, C. A 19.0% efficiency achieved in CuO_x-based inverted $CH_3NH_3PbI_{3-x}Cl_x$ solar cells by an effective Cl doping method. *Nano Energy* **2016**, *27*, 51–57. [CrossRef]

37. Igbari, F.; Li, M.; Hu, Y.; Wang, Z.-K.; Liao, L.-S. A room temperature $CuAlO_2$ hole interfacial layer for efficient and stable planar perovskite solar cells. *J. Mater. Chem. A* **2016**, *4*, 1326–1335. [CrossRef]

38. Chen, Y.; Yang, Z.; Wang, S.; Zheng, X.; Wu, Y.; Yuan, N.; Zhang, W.-H.; Liu, S.F. Design of an inorganic mesoporous hole-transporting layer for highly efficient and stable inverted perovskite solar cells. *Adv. Mater.* **2018**, *30*, 1805660. [CrossRef]

39. Qin, P.; He, Q.; Yang, G.; Yua, X.; Xiong, L.; Fang, G. Metal ions diffusion at heterojunction chromium oxide/$CH_3NH_3PbI_3$ interface on the stability of perovskite solar cells. *Surf. Interfaces* **2018**, *10*, 93–99. [CrossRef]

40. Li, D.; Tong, C.; Ji, W.; Fu, Z.; Wan, Z.; Huang, Q.; Ming, Y.; Mei, A.; Hu, Y.; Rong, Y.; et al. Vanadium oxide post-treatment for enhanced photovoltage of printable perovskite solar cells. *ACS Sustain. Chem. Eng.* **2019**, *7*, 2619–2625. [CrossRef]

41. Shalan, A.E.; Oshikiri, T.; Narra, S.; Elshanawany, M.M.; Ueno, K.; Wu, H.-P.; Nakamura, K.; Shi, X.; Diau, E.W.-G.; Misawa, H. Cobalt oxide (CoO$_x$) as an efficient hole-extracting layer for high-performance inverted planar perovskite solar cells. *ACS Appl. Mater. Interfaces* **2016**, *8*, 33592–33600. [CrossRef]

42. Im, K.; Heo, J.H.; Im, S.H.; Kim, J.S. Scalable synthesis of Ti-doped MoO$_2$ nanoparticle-hole-transporting material with high moisture stability for CH$_3$NH$_3$PbI$_3$ perovskite solar cells. *Chem. Eng. J.* **2017**, *330*, 698–705. [CrossRef]

43. Lee, B.; Shin, B.; Park, B. Uniform Cs$_2$SnI$_6$ thin films for lead-free and stable perovskite optoelectronics via hybrid deposition approaches. *Electron. Mater. Lett.* **2019**, *15*, 192–200. [CrossRef]

44. Chen, W.-C.; Tunuguntla, V.; Chiu, M.-H.; Li, L.-J.; Shown, I.; Lee, C.-H.; Hwang, J.-S.; Chen, L.-C.; Chen, K.-H. Co-solvent effect on microwave-assisted Cu$_2$ZnSnS$_4$ nanoparticles synthesis for thin film solar cell. *Sol. Energy Mater. Sol. Cells* **2017**, *161*, 416–423. [CrossRef]

45. Li, D.; Fang, X.; Deng, Z.; Zhou, S.; Tao, R.; Dong, W.; Wang, T.; Zhao, Y.; Meng, G.; Zhu, X. Electrical, optical and structural properties of CuCrO$_2$ films prepared by pulsed laser deposition. *J. Phys. D Appl. Phys.* **2007**, *40*, 4910–4915. [CrossRef]

46. Wang, J.; Zheng, P.; Li, D.; Deng, Z.; Dong, W.; Tao, R.; Fang, X. Preparation of delafossite-type CuCrO$_2$ films by Sol–Gel method. *J. Alloys Compd.* **2011**, *509*, 5715–5719. [CrossRef]

47. Xiong, D.; Xu, Z.; Zeng, X.; Zhang, W.; Chen, W.; Xu, X.; Wang, M.; Cheng, Y.-B. Hydrothermal synthesis of ultrasmall CuCrO$_2$ nanocrystal alternatives to NiO nanoparticles in efficient p-Type dye-sensitized solar cells. *J. Am. Chem.* **2012**, *22*, 24760–24768. [CrossRef]

48. Yu, R.-S.; Wu, C.-M. Characteristics of p-Type transparent conductive CuCrO$_2$ thin films. *Appl. Surf. Sci.* **2013**, *282*, 92–97. [CrossRef]

49. Barnabé, A.; Thimont, Y.; Lalanne, M.; Presmanesa, L.; Tailhades, P. p-Type conducting transparent characteristics of delafossite Mg-doped CuCrO$_2$ thin films prepared by RF-Sputtering. *J. Mater. Chem. C* **2015**, *3*, 6012–6024. [CrossRef]

50. Sánchez-Alarcón, R.I.; Oropeza-Rosario, G.; Gutierrez-Villalobos, A.; Muro-López, M.A.; Martínez-Martínez, R.; Zaleta-Alejandre, E.; Falcony, C.; Alarcón-Flores, G.; Fragoso, E.; Hernández-Silva, O.; et al. Ultrasonic spray-pyrolyzed CuCrO$_2$ thin films. *J. Phys. D Appl. Phys.* **2016**, *49*, 175102. [CrossRef]

51. Nie, S.; Liu, A.; Meng, Y.; Shin, B.; Liu, G.; Shan, F. Solution processed ternary p-Type CuCrO$_2$ semiconductor thin films and their application in transistors. *J. Mater. Chem. C* **2018**, *6*, 1393–1398. [CrossRef]

52. Dunlap-Shohl, W.A.; Daunis, T.B.; Wang, X.; Wang, J.; Zhang, B.; Barrera, D.; Yan, Y.; Hsu, J.W.P.; Mitzi, D.B. Room-temperature fabrication of a delafossite CuCrO$_2$ hole transport layer for perovskite solar cells. *J. Mater. Chem. A* **2018**, *6*, 469–477. [CrossRef]

53. Zhang, H.; Wang, H.; Zhu, H.; Chueh, C.-C.; Chen, W.; Yang, S.; Jen, A.K.-Y. Low-temperature solution-processed CuCrO$_2$ hole-transporting layer for efficient and photostable perovskite solar cells. *Adv. Energy Mater.* **2018**, *8*, 1702762. [CrossRef]

54. Jeong, S.; Seo, S.; Shin, H. p-Type CuCrO$_2$ particulate films as the hole transporting layer for CH$_3$NH$_3$PbI$_3$ perovskite solar cells. *RSC Adv.* **2018**, *8*, 27956–27962. [CrossRef]

55. Yang, B.; Ouyang, D.; Huang, Z.; Ren, X.; Zhang, H.; Choy, W.C.H. Multifunctional synthesis approach of n: CuCrO$_2$ nanoparticles for hole transport layer in high-performance perovskite solar cells. *Adv. Funct. Mater.* **2019**, *29*, 1902600. [CrossRef]

56. Akin, S.; Liu, Y.; Dar, M.I.; Zakeeruddin, S.M.; Grätzel, M.; Turand, S.; Sonmezoglu, S. Hydrothermally processed CuCrO$_2$ nanoparticles as an inorganic hole transporting material for low cost perovskite solar cells with superior stability. *J. Mater. Chem. A* **2018**, *6*, 20327–20337. [CrossRef]

57. Cao, J.; Yu, H.; Zhou, S.; Qin, M.; Lau, T.-K.; Lu, X.; Zhao, N.; Wong, C.-P. Low-temperature solution-processed NiO$_x$ films for air-stable perovskite solar cells. *J. Mater. Chem. A* **2017**, *5*, 11071–11077. [CrossRef]

58. Mali, S.S.; Patil, J.V.; Kim, H.; Luque, R.; Hong, C.K. Highly efficient thermally stable perovskite solar cells via Cs:NiO$_x$/CuSCN double-inorganic hole extraction layer interface engineering. *Mater. Today* **2019**, *26*, 8–18. [CrossRef]

59. Lee, B.; Yun, A.J.; Kim, J.; Gil, B.; Shin, B.; Park, B. Aminosilane-Modified CuGaO$_2$ Nanoparticles incorporated with CuSCN as a hole-transport layer for efficient and stable perovskite solar cells. *Adv. Mater. Interfaces* **2019**, *6*, 1901372. [CrossRef]

60. Panidi, J.; Paterson, A.F.; Khim, D.; Fei, Z.; Han, Y.; Tsetseris, L.; Vourlias, G.; Patsalas, P.A.; Heeney, M.; Anthopoulos, T.D. Remarkable enhancement of the hole mobility in several organic small-molecules, polymers, and small-molecule: Polymer blend transistors by simple admixing of the lewis acid p-dopant B(C$_6$F$_5$)$_3$. *Adv. Sci.* **2018**, *5*, 1700190. [CrossRef]

61. Pitchaiya, S.; Natarajan, M.; Santhanam, A.; Asokan, V.; Yuvapragasam, A.; Ramakrishnan, V.M.; Palanisamy, S.E.; Sundaram, S.; Velauthapillai, D. A review on the classification of organic/inorganic/carbonaceous hole transporting materials for perovskite solar cell application. *Arab. J. Chem.* **2020**, *13*, 2526–2557. [CrossRef]

62. Kim, J.I.; Kim, J.; Lee, J.; Jung, D.-R.; Kim, H.; Choi, H.; Lee, S.; Byun, S.; Kang, S.; Park, B. Photoluminescence enhancement in CdS quantum dots by thermal annealing. *Nanoscale Res. Lett.* **2012**, *7*, 482. [CrossRef]

63. Chen, J.; Kim, S.-G.; Ren, X.; Jung, H.S.; Park, N.-G. Effect of bidentate and tridentate additives on the photovoltaic performance and stability of perovskite solar cells. *J. Mater. Chem. A* **2019**, *7*, 4977–4987. [CrossRef]

64. Han, G.; Hadi, H.D.; Bruno, A.; Kulkarni, S.A.; Koh, T.M.; Wong, L.H.; Soci, C.; Mathews, N.; Zhang, S.; Mhaisalkar, S.G. Additive selection strategy for high performance perovskite photovoltaics. *J. Phys. Chem. C* **2018**, *122*, 13884–13893. [CrossRef]

65. Kim, Y.; Jung, E.H.; Kim, G.; Kim, D.; Kim, B.J.; Seo, J. Sequentially fluorinated PTAA polymers for enhancing V_{OC} of high-performance perovskite solar cells. *Adv. Energy Mater.* **2018**, *8*, 1801668. [CrossRef]

66. Kim, J.; Lee, Y.; Yun, A.J.; Gil, B.; Park, B. Interfacial modification and defect passivation by the cross-linking interlayer for efficient and stable CuSCN-based perovskite solar cell. *ACS Appl. Mater. Interfaces* **2019**, *11*, 46818–46824. [CrossRef] [PubMed]

67. Bube, R.H. Trap density determination by space-charge-limited currents. *J. Appl. Phys.* **1962**, *33*, 1733–1737. [CrossRef]

68. Guerrero, A.; Garcia-Belmonte, G.; Mora-Sero, I.; Bisquert, J.; Kang, Y.S.; Jacobsson, T.J.; Correa-Baena, J.-P.; Hagfeldt, A. Properties of contact and bulk impedances in hybrid lead halide perovskite solar cells including inductive loop elements. *J. Phys. Chem. C* **2016**, *120*, 8023–8032. [CrossRef]

69. Kim, J.; Hwang, T.; Lee, S.; Lee, B.; Kim, J.; Kim, J.; Gil, B.; Park, B. Synergetic effect of double-step blocking layer for the perovskite solar cell. *J. Appl. Phys.* **2017**, *122*, 145106. [CrossRef]

70. Lee, S.; Flanagan, J.C.; Lee, B.; Hwang, T.; Kim, J.; Gil, B.; Shim, M.; Park, B. Route to improving photovoltaics based on CdSe/CdSe$_x$Te$_{1-x}$ type-ii heterojunction nanorods: The effect of morphology and cosensitization on carrier recombination and transport. *ACS Appl. Mater. Interfaces* **2017**, *9*, 31931–31939. [CrossRef]

71. Lee, S.; Flanagan, J.C.; Kim, J.; Yun, A.J.; Lee, B.; Shim, M.; Park, B. Efficient type-ii heterojunction nanorod sensitized solar cells realized by controlled synthesis of core/patchy-shell structure and CdS cosensitization. *ACS Appl. Mater. Interfaces* **2019**, *11*, 19104–19114. [CrossRef]

72. Almora, O.; Aranda, C.; Mas-Marzá, E.; Garcia-Belmonte, G. On mott-schottky analysis interpretation of capacitance measurements in organometal perovskite solar cells. *Appl. Phys. Lett.* **2016**, *109*, 173903. [CrossRef]

73. Gunawan, O.; Gokmen, T.; Warren, C.W.; Cohen, J.D.; Todorov, T.K.; Barkhouse, D.A.R.; Bag, S.; Tang, J.; Shin, B.; Mitzi, D.B. Electronic properties of the Cu$_2$ZnSn(Se,S)$_4$ absorber layer in solar cells as revealed by admittance spectroscopy and related methods. *Appl. Phys. Lett.* **2012**, *100*, 253905. [CrossRef]

74. Walter, T.; Herberholz, R.; Müller, C.; Schock, H.W. Determination of defect distributions from admittance measurements and application to Cu(In,Ga)Se$_2$ based heterojunctions. *J. Appl. Phys.* **1996**, *80*, 4411–4420. [CrossRef]

75. Reese, M.O.; Gevorgyan, S.A.; Jørgensen, M.; Bundgaard, E.; Kurtz, S.R.; Ginley, D.S.; Olson, D.C.; Lloyd, M.T.; Moryillo, P.; Katz, E.A.; et al. Consensus stability testing protocols for organic photovoltaic materials and devices. *Sol. Energy Mater. Sol. Cells* **2011**, *95*, 1253–1267. [CrossRef]

76. Domanski, K.; Alharbi, E.A.; Hagfeldt, A.; Grätzel, M.; Tress, W. Systematic investigation of the impact of operation conditions on the degradation behaviour of perovskite solar cells. *Nat. Energy* **2018**, *3*, 61–67. [CrossRef]

77. Hwang, T.; Yun, A.J.; Kim, J.; Cho, D.; Kim, S.; Hong, S.; Park, B. Electronic traps and their correlations to perovskite solar cell performance via compositional and thermal annealing controls. *ACS Appl. Mater. Interfaces* **2019**, *11*, 6907–6917. [CrossRef]

78. Yun, A.J.; Kim, J.; Hwang, T.; Park, B. Origins of efficient perovskite solar cells with low-temperature processed SnO$_2$ electron transport layer. *ACS Appl. Energy Mater.* **2019**, *2*, 3554–3560. [CrossRef]

79. Ni, Z.; Bao, C.; Liu, Y.; Jiang, Q.; Wu, W.-Q.; Chen, S.; Dai, X.; Chen, B.; Hartweg, B.; Yu, Z.; et al. Resolving spatial and energetic distributions of trap states in metal halide perovskite solar cells. *Science* **2020**, *367*, 1352–1358. [CrossRef]

80. Hwang, T.; Yun, A.J.; Lee, B.; Kim, J.; Lee, Y.; Park, B. Methylammonium-chloride post-treatment on perovskite surface and its correlation to photovoltaic performance in the aspect of electronic traps. *J. Appl. Phys.* **2019**, *126*, 023101. [CrossRef]

81. Tan, W.; Bowring, A.R.; Meng, A.C.; McGehee, M.D.; McIntyre, P.C. Thermal stability of mixed cation metal halide perovskites in air. *ACS Appl. Mater. Interfaces* **2018**, *10*, 5485–5491. [CrossRef]

82. Szostak, R.; Silva, J.C.; Turren-Cruz, S.-H.; Soares, M.M.; Freitas, R.O.; Hagfeldt, A.; Tolentino, H.C.N.; Nogueira, A.F. Nanoscale mapping of chemical composition in organic-inorganic hybrid perovskite films. *Sci. Adv.* **2019**, *5*, eaaw6619. [CrossRef] [PubMed]

83. Seo, J.-Y.; Kim, H.-S.; Akin, S.; Stojanovic, M.; Simon, E.; Fleischer, M.; Hagfeldt, A.; Zakeeruddin, S.M.; Grätzel, M. Novel p-dopant toward highly efficient and stable perovskite solar cells. *Energy Environ. Sci.* **2018**, *11*, 2985–2992. [CrossRef]